AGU PUBLICATIONS

Geophysical Research Letters

RESEARCH LETTER
10.1002/2015GL063325

Key Points:
- AOD and soil moisture showed a negative exponential relationship
- The effects of soil moisture on AOD increase under strong wind speed conditions
- The criteria of AOD for dust-outbreak controls thresholds of VSM and WS

Correspondence to:
M. Choi,
mhchoi@skku.edu

Citation:
Kim, H., and M. Choi (2015), Impact of soil moisture on dust outbreaks in East Asia: Using satellite and assimilation data, *Geophys. Res. Lett.*, *42*, doi:10.1002/2015GL063325.

Received 30 JAN 2015
Accepted 20 MAR 2015
Accepted article online 24 MAR 2015

Impact of soil moisture on dust outbreaks in East Asia: Using satellite and assimilation data

Hyunglok Kim[1] and Minha Choi[1]

[1]Water Resources and Remote Sensing Laboratory, Department of Water Resources, Graduate School of Water Resources, Sungkyunkwan University, Suwon, South Korea

Abstract This study is the first assessment of the effects of soil moisture on dust outbreaks using satellite-derived aerosol optical depth (AOD) and global assimilation data on the sand regions across East Asia. The relationships among dust outbreaks, soil moisture, and wind speed were estimated using data sets of the Moderate Resolution Imaging Spectroradiometer and Global Land Data Assimilation System collected over 11 years (2003–2013). The mean AOD exponentially decreased with increasing soil moisture under different wind speed conditions (average determination coefficient = 0.95). As the wind speed conditions became stronger, the probability of a dust outbreak became greatly affected by soil moisture. The threshold soil moisture for dust outbreaks increased with increasing wind speed and decreased with increasing dust-outbreak criteria of AOD. Our results have the capability to be applied to satellite-based dust-outbreak prediction and global-scale dust-emission studies.

1. Introduction

Sand dust has direct implications for public health, transportation, and agriculture, with indirect effects on climate through modification of the microphysical properties of clouds [*Zhang and Carmichael*, 1999; *Kwon et al.*, 2002; *Tegen*, 2003; *Bangert et al.*, 2012]. In addition, it is considered one of the major sources of the tropospheric aerosol component, which plays an important role in climate systems and affects the atmospheric radiation budget by scattering and absorbing longwave and shortwave radiation [*Sokolik and Toon*, 1996; *Tegen et al.*, 1996; *Kaufman et al.*, 2002; *Myhre et al.*, 2003].

Surface wind speed has generally been regarded as the main factor determining the mobilization of sand and dust in dust-source regions [*Chomette et al.*, 1999]. However, dust events are influenced not only by wind speed but also by surface conditions [*Ravi et al.*, 2004; *Natsagdorj et al.*, 2003; *Wang et al.*, 2004; *Ishizuka et al.*, 2005; *Tegen et al.*, 2004; *Cowie et al.*, 2013]. Surface conditions such as soil moisture determine the threshold friction velocity for a dust outbreak on bare soil, except in conditions of extreme cold or in the presence of coarse soil particles, because soil moisture increases the cohesive forces between soil particles; therefore, moistened sand requires higher wind speed to generate a dust event, especially under humid conditions.

Many efforts have been made in laboratories and observatories to elucidate the mechanisms of dust emissions from moistened sand [*Gillette et al.*, 1982; *Fécan et al.*, 1999; *Dong et al.*, 2002; *Ravi and D'Odorico*, 2005]. However, such research has limited application for estimating the relationship between soil moisture on a global scale, and for natural dust events. To understand the mechanisms linking dust events and soil moisture trends on a global scale, employment of satellite-based and global assimilation data would be required.

With the development of satellite remote sensing and data-assimilating techniques, application to several hydrological research fields has been achieved [*Crow and Ryu*, 2009; *Kerr et al.*, 2010; *Chen et al.*, 2013]. In dust research, satellite remote sensing has provided a powerful tool for characterization of global dust properties, and the aerosol product data obtained provide more objective and quantitative measurement criteria than visibility inspection by the human eye [*Sokolik*, 2002; *Prospero et al.*, 2002; *Schepanski et al.*, 2007; *Baddock et al.*, 2009; *Parajuli et al.*, 2014]. Moreover, data-assimilating techniques (i.e., Global Land Data Assimilation System (GLDAS)) allow assessment of global land surface conditions through integration of satellite- and ground-based data and use of several land surface models.

In the present study, satellite-derived aerosol products and global assimilation data were linked to estimate the effect of soil moisture on dust phenomena over sand areas in East Asia. Through this analysis, the following

were characterized: (1) the relationships among volumetric soil moisture (0–10 cm), wind speed, and aerosol optical depth; (2) dust-outbreak possibilities and threshold soil moisture; and (3) the effect of soil moisture on dust outbreaks and threshold wind speed.

2. Data Sets

2.1. Aerosol Products

The Moderate Resolution Imaging Spectroradiometer (MODIS) sensors aboard the Earth Observing System Terra and Aqua polar orbiter platforms are specially designed to analyze atmospheric (i.e., cloud and aerosol) and land properties (i.e., surface reflectance and evapotranspiration) with reliable accuracy. MODIS deep blue 550 nm aerosol optical depth (AOD) data were selected for this study because these data have already been extensively validated by several researchers in field studies. Moreover, deep blue data maintain accuracy even over bright desert surfaces, whereas other satellite-based algorithms have difficulty obtaining accurate reading [*Ginoux et al*., 2012]. For details about the Deep Blue algorithm, please refer to *Hsu et al*. [2004]. Level 2 MODIS deep blue AOD (Aqua) products reported daily at noon at a spatial resolution of $0.01° \times 0.01°$ are available for 2003 to the present. Herein, the level 2 AOD data were resampled to a spatial resolution of $0.25° \times 0.25°$ to match the resolution of the Global Land Data Assimilation System (GLDAS).

2.2. Land Surface Products

GLDAS has used several satellites (i.e., NOAA, Terra, and Tropical Rainfall Measuring Mission), and ground-based data set (i.e., Climate Prediction Center Merged Analysis of Precipitation, National Centers for Environmental Prediction, and National Center for Atmospheric Research) in order to characterize the state of the land surface [*Rodell et al*., 2004; *Sheffield et al*., 2006]. GLDAS products have been widely analyzed at a spatial resolution from $0.25° \times 0.25°$ to $1° \times 1°$ [*Chen et al*., 2013]. In particular, GLDAS products are commonly used as reference values for validation of satellite-retrieved soil moisture contents [*Dorigo et al*., 2010]. GLDAS/Noah products reported every 3 h at a spatial resolution of $0.25° \times 0.25°$ are available for 2000 to the present. In the analyses, wind speed (WS) at 10.0 m height, volumetric soil moisture (VSM), and soil temperature at a depth of 0–10.0 cm, and rainfall rate from GLDAS data were employed, with times proximate to MODIS AOD retrieval.

2.3. Land Properties

The Harmonized World Soil Database (HWSD) is a raster database at a spatial resolution of 1 km with more than 16,000 different soil texture mapping units. It combines existing regional and national updates on soil information, with a 1:5,000,000 scale Food and Agriculture Organization-United Nations Educational, Scientific and Cultural Organization Soil Map of the World. The HWSD consists of 221 million grid cells covering the globe's land territory, and it has been used in the identification of dust sources, as well as for and applied in many other research fields [e.g., *Saxton and Rawls*, 2006; *Batjes*, 2009; *FAO/IIASA/ISRIC/ISS-CAS/JRC*, 2009].

3. Methodology

In this study, sand areas were defined using the U.S. Department of Agriculture (USDA) topsoil texture classifications from the HWSD data sets. Figure 1 shows the spatial distribution of the East Asian sand fraction. Sand fraction pixels indicating a sand fraction of more than 80% were classified as sand areas. These include many famous bare deserts in East Asia already known to be major dust-source regions [*Wang et al*., 2004; *Sun et al*., 2001].

To allow accurate analysis of the effects of soil moisture on dust outbreaks, several specific conditions were excluded. First, pixels below 0°C were masked for occurrence of frost- and snow-covered sand areas. Second, days on which precipitation occurred were excluded to avoid use of instantaneous AOD data detected just before and after rainfall events. Third, the fine mode aerosol caused by transported dust or biomass burning was eliminated using the threshold of an Angström Exponent larger than 0.35 [*Eck et al*., 1999; *Parajuli et al*., 2014]. With these exclusions in place, we assembled 11 years of AOD, VSM, and WS data, each with $0.25° \times 0.25°$ grid cells over the East Asian sand areas from the MODIS and GLDAS data. From the East Asian sand areas (6790 pixels), a total of 27.261 million data points were employed in the analysis.

To allow simultaneous consideration of various VSM and WS conditions, we divided the VSM range at 1.0% intervals and WS at 1.0 ms^{-1} intervals. Through this combination ($_{375}C_2$), 375 groups of ranged VSM (5.0 to less

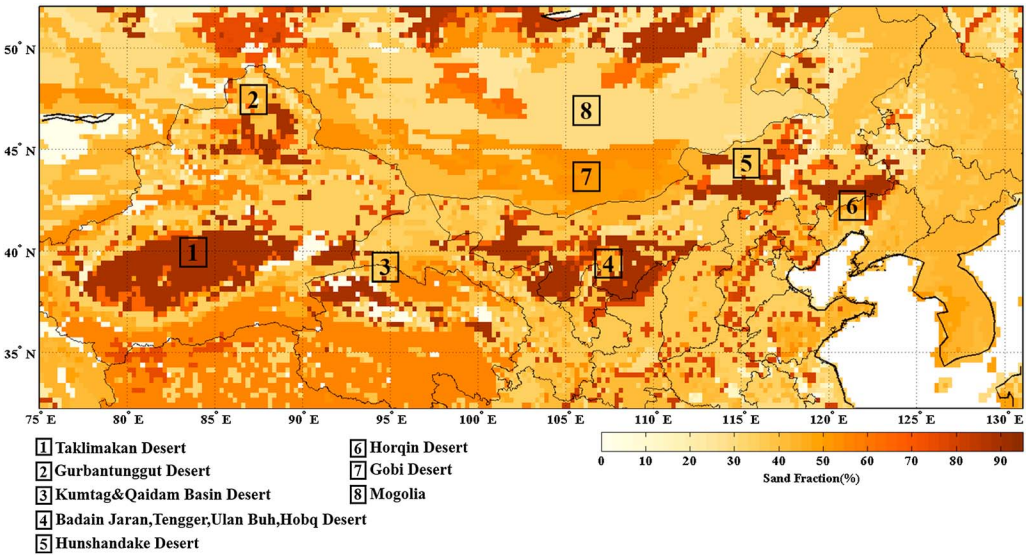

Figure 1. Sand fraction over East Asia, based on Harmonized World Soil Database (HWSD). Most areas have more than 80% sand fraction (#1 to #6, 6790 pixels total), classified as sand by the USDA classification. Areas #1 to #8 show well-known dust sources in East Asia.

than 30.0%) and ranged WS (0.0 to less than 15.0 ms^{-1}) were obtained. The general VSM values ranged from 5.0% to 26.0% over the East Asian sand regions during the 11 years of the study period.

4. Results and Discussion

4.1. Strong Wind Speed and AOD

Figure 2 shows the monthly variation of the total number of AOD at 0.5 interval and the total number of strong wind speed occurrences during 11 years. Strong wind speed is commonly used in dust research to explain dust outbreaks [*Kurosaki and Mikami*, 2003]. To estimate the relationship between strong wind speed and AOD, a specific AOD value was designed as the dust-outbreak state using criteria from the previous research of *Park*

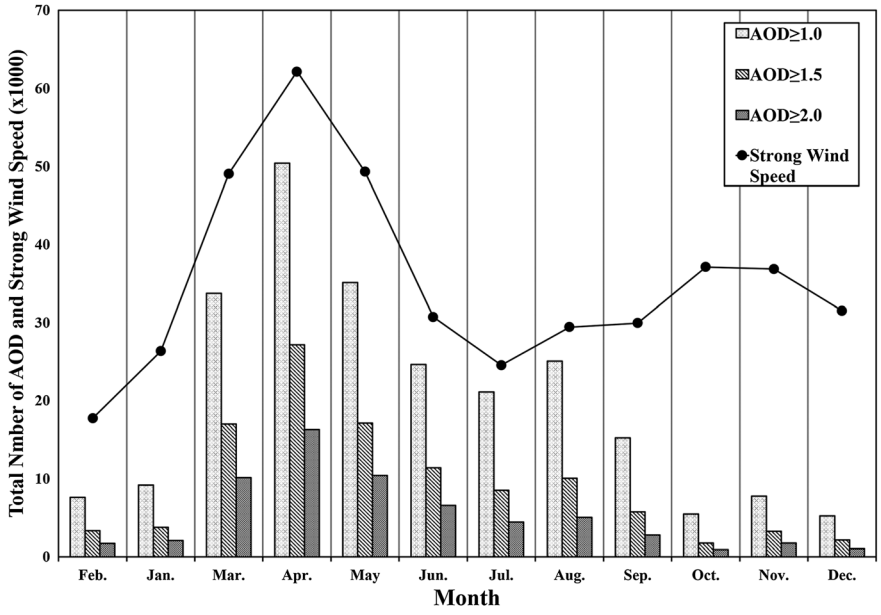

Figure 2. Variation of total number of strong wind speed (≥6.5 ms^{-1}), $AOD_{\geq 1.0}$, $AOD_{\geq 1.5}$, and $AOD_{\geq 2}$.0 occurrences in different months for 11 years over the East Asian sand regions.

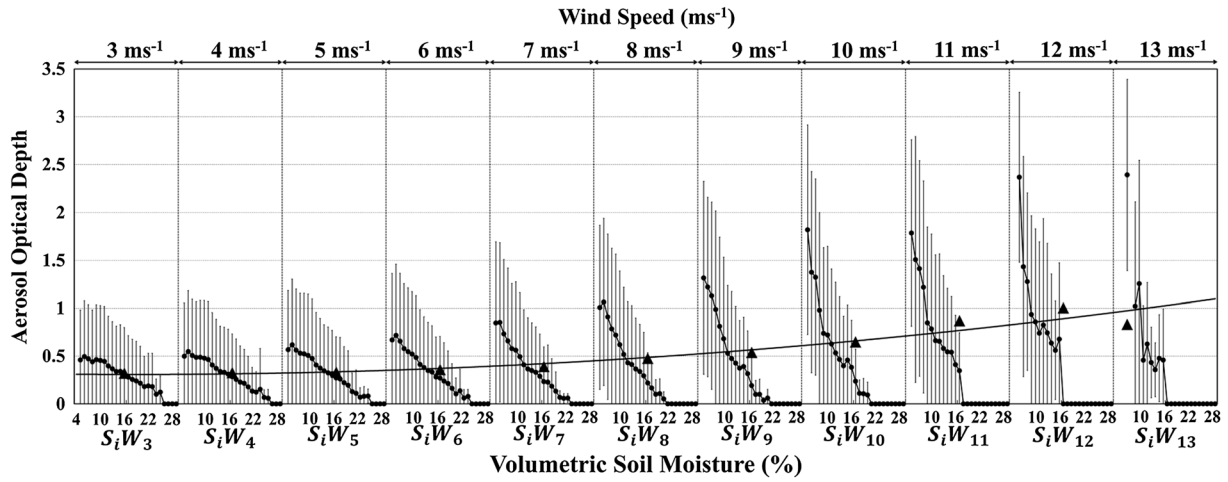

Figure 3. The relationships among AOD, WS, and VSM. *Y* axis shows AOD values under different S_iW_j conditions. Black dots indicate mean AOD value under S_iW_j conditions. The gray line for each dot indicates standard deviation. Black triangles represent averaged AOD values under different wind speed conditions (upper *x* axis).

et al. [2014]. According to *Park et al*. [2014], AOD values from 1.0 to 3.0 represent the dust-outbreak state. Strong wind speeds and AOD values higher than 1.0, 1.5, and 2.0 were found to have high correlation coefficient values of 0.76, 0.80, and 0.83, respectively. This suggested that high AOD_{range} (AOD_{range} represents an AOD higher than a specific *range*) could be used as a reasonable criterion for defining dust outbreaks. These results supported the findings of *Kurosaki and Mikami* [2003], which showed the tendency of correlation between strong wind speed and dust outbreak frequency. This indicates that the linking of satellite-based data with assimilation data can be employed for diverse dust-related research on a regional scale.

4.2. Relationships Among AOD, Soil Moisture, and Wind Speed

Figure 3 represents an AOD under a condition grid cell with VSM ranging from *i* to $(i+1)$ (%), and WS from *j* to $(j+1)$ ms^{-1} along the bottom of the *x* axis (S_iW_j). For statistical analysis, the S_iW_j groups for which less than 25 samples were available were rejected. For example, S_9W_5 denotes a condition grid cell with a VSM of 9.0 to 10.0% and a WS of 5.0 to 6.0 ms^{-1}. To give a better understanding, the S_iW_3 *x* axis zone shows WS fixed at 3.0 to 4.0 ms^{-1} (upper *x* axis) with VSM ranging from 5.0 to 30.0% (lower *x* axis). Without considering the effect of soil moisture, the mean AOD climbed steadily with increasing WS (black solid line and upper *x* axis). However, when the effect of soil moisture was applied to the relationship between AOD and WS, the mean AOD under S_iW_j condition $\left(AOD_{mean|S_iW_j}\right)$ varied significantly with soil moisture in different WS conditions (black dots, lower *x* axis). As expected, most $AOD_{mean|S_iW_j}$ showed a decreasing pattern with increasing soil moisture. In order to lift the sand particles containing higher moistures, stronger wind speed is required to overcome the cohesive strength between soil particles.

4.3. Exponential Relationship Between AOD and Soil Moisture

Further investigation into the AOD, VSM, and WS relationships is depicted in Figure 4. An exponential decrease of $AOD_{mean|S_iW_j}$ was observed with increasing soil moisture under different WS conditions. This relationship can be explained by equation (1).

$$AOD_{mean|S_iW_j} = C_1 \cdot \exp(-C_2 \cdot VSM) \quad (1)$$

Each $AOD_{mean|S_iW_j}$ regression function had a high R^2 value (0.83 to 0.98), low root-mean-square error value (0.23 to 0.02), and low sum of squared errors value (0.01 to 0.48) (Figure 4). The constants C_1 and C_2 varied with WS conditions. Equation (1) and Figure 4 illustrate that given a fixed VSM, the variation of $AOD_{mean|S_iW_j}$ increased as WS became stronger. In fixed WS conditions (fixed C_1 and C_2), however, the variation of $AOD_{mean|S_iW_j}$ decreased as VSM increased. Higher $AOD_{mean|S_iW_j}$ variation is therefore associated with higher WS and lower VSM. However, under wet conditions (VSM larger than about 16%), the $AOD_{mean|S_iW_j}$ values were barely affected by WS conditions.

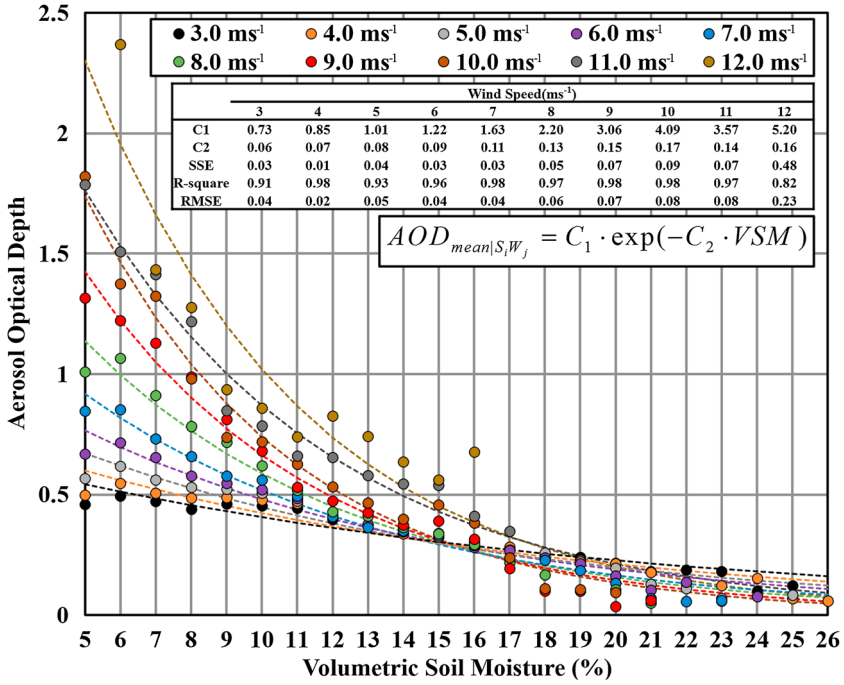

Figure 4. The relationship of averaged AOD and VSM under different wind speed conditions. The upper part of the graph indicates stronger wind speed conditions. Constants (C_1 and $C2$) and statistical information for each line are included.

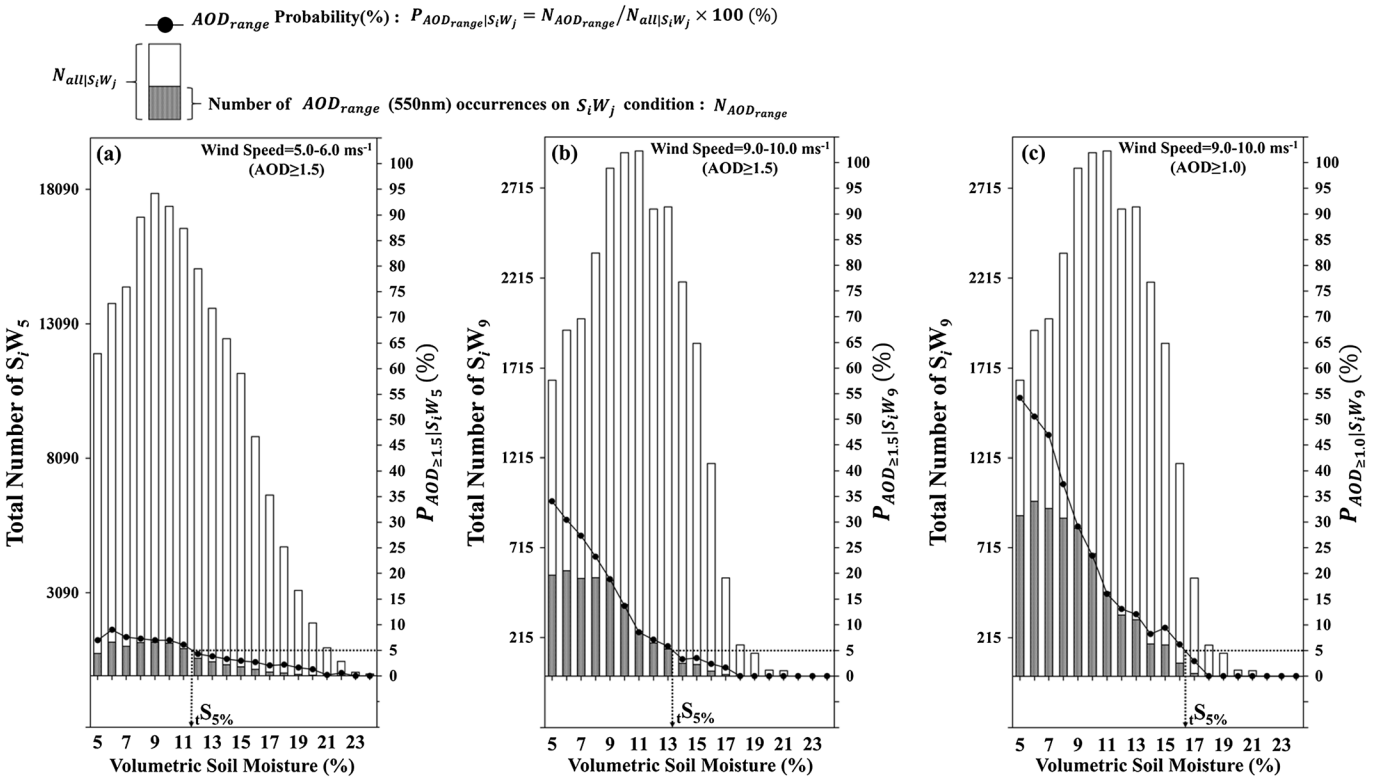

Figure 5. (a–c) Each bar graph shows the total number of S_iW_j over East Asian sand areas from 2003 to 2013. Gray bars indicate the total number of specific ranged-AOD occurrences under S_iW_j conditions $\left(N_{\mathrm{AOD}_{\mathrm{range}}}\right)$. The bar height indicates the total number of S_iW_j conditions $\left(N_{\mathrm{all}|S_iW_j}\right)$. The black line graph shows the specific range of AOD occurrence probability given a particular S_iW_j condition.

Table 1. DPSD[a] and $tS_{5\%}$[b] Under Different S_iW_j Conditions With the Dust Outbreak Criterion of 1.5 AOD

	S_iW_j									
	S_iW_3	S_iW_4	S_iW_5	S_iW_6	S_iW_7	S_iW_8	S_iW_9	S_iW_{10}	S_iW_{11}	S_iW_{12}
DPSD (%)	1.5	2.1	2.8	3.9	5.5	8.2	11.6	16.9	19.1	25.5
$tS_{5\%}$ (%)	11.1	11.6	11.7	11.9	12.0	13.2	13.3	13.4	15.4	18.0

[a]The dust-outbreak probability standard deviation.
[b]The threshold of VSM for a dust outbreak (GLDAS 0–10 cm volumetric soil moisture).

4.4. Statistically Estimated Dust Event Probability and Soil Moisture Threshold

In Figure 5, the height of the bar indicates the total number of S_iW_j conditions $\left(N_{\text{all}|S_iW_j}\right)$, while the height of the gray bar indicates the total number of occurrences of $\text{AOD}_{\text{range}}$ within the S_iW_j conditions ($N_{\text{AOD range}}$) over the East Asian sand areas from 2003 to 2013. The black line indicates the $\text{AOD}_{\text{range}}$ probability for a sand area under S_iW_j condition, calculated using equation (2).

$$P_{\text{AOD}_{\text{range}}|S_iW_j} = N_{\text{AOD}_{\text{range}}}/N_{\text{all}|S_iW_j} \times 100(\%) \tag{2}$$

This method was suitable because the satellite data had coarse temporal resolution characteristics. This statistical procedure was also used in previous studies [e.g., *Kurosaki et al*., 2011]. In Figure 5a, under S_iW_5 condition, VSM and the dust-outbreak probability are denoted when the dust-outbreak criterion is 1.5 AOD. In lower WS conditions (Figure 5a, S_iW_5), little change of the dust-outbreak probability was observed with variation of VSM. In this condition, the dust-outbreak probability standard deviation (DPSD) value was only about 2.8%. In a higher wind speed condition (Figure 5b, S_iW_9), the DPSD value of 11.6% was observed (Table 1). The DPSD results indicated that dust-outbreak probabilities are highly affected by wind speed and soil moisture conditions. Moreover, the threshold VSM for the dust-emission value was determined using the concept of the most favorable state for dust outbreak from *Kurosaki and Mikami* [2007]. The threshold VSM for dust outbreak represents the maximum value of VSM at which a dust outbreak can occur. The threshold VSM may have significant application for global-scale dust-outbreak prediction and sediment transport functions [*Dong et al*., 2002]. The threshold VSM for dust outbreaks ($tS_{5\,\%}$) increased with WS (Table 1). This result was similar to those of several previous studies [e.g., *Fécan et al*., 1999; *Ishizuka et al*., 2005], but the present research expanded the scale from the laboratory or observatory to examination of the natural state of an area. Figures 5b and 5c applied the same S_iW_j conditions; however, in Figure 5c the dust-outbreak criterion decreased from 1.5 to 1.0 AOD. Therefore, the DPSD value increased from 11.6 to 22.0%, and $tS_{5\,\%}$ increased from 13.3 to 16.5% (Table 1 and Figure 5). The physical reasoning for the increased $tS_{5\,\%}$ is that higher soil moisture content is required in order to increase the capillary forces between soil particles to prevent emission from the source area for less dusty conditions under the same WS condition. Moreover, this result illustrates how, like recording dust outbreaks by human eye judgment, different choices in setting the criterion of a dust outbreak (AOD value) can lead to seriously differences in the dust-outbreak threshold WS and VSM values. This discrepancy is one of the main explanations for the differing threshold results between studies [*Engelstaedter et al*., 2003].

5. Conclusion

Using 11 years of satellite-based data and global assimilation data sets, the effect of soil moisture on dust outbreaks was examined. Previous research depended on laboratory- and observatory-scale data, which have limited value when considering the effects of soil moisture in dust outbreaks on a global scale. Thanks to the development of satellite remote sensing and data-assimilating technology, we were able to consider global-scale soil moisture data for evaluation of dust outbreaks. The following observations were made:

1. We found a positive correlation between strong wind speed ($\geq$6.5 ms^{-1}) and high $\text{AOD}_{\text{range}}$ frequency, which we took to indicate a state of dust outbreak.
2. The East Asian sand area $\text{AOD}_{\text{mean}|S_iW_j}$ and soil moisture showed a negative exponential relationship under different wind speed conditions. A higher $\text{AOD}_{\text{mean}|S_jW_i}$ variation rate was associated with higher wind speeds and lower soil moisture contents.

3. Soil moisture had little effect on the dust-outbreak probability under low wind speed conditions. In contrast, it highly affected the dust-outbreak probability under stronger wind speed conditions.
4. The threshold soil moisture for dust outbreak ($tS_{5\,\%}$) increased with increasing wind speed.
5. The threshold value for dust outbreak showed considerable variation with different values for the criterion of dust outbreak.

This first attempt to derive the dust-outbreak possibilities and threshold soil moisture using satellite-based and assimilation data ($0.25° \times 0.25°$ pixel scale) demonstrated the potential of determining the effects of soil moisture on dust phenomena beyond laboratory- and observatory-scale analyses. However, the current results are only valid for bare sand areas. Therefore, the soil moisture variation for other types of soil (e.g., silt and clay) and vegetation dynamics (e.g., normalized difference vegetation index) needs to be considered in future research.

Acknowledgments
This research was supported by the Space Core Technology Development Program through the National Research Foundation of Korea (NRF), funded by the Ministry of Science, ICT and Future Planning (NRF-2014M1A3A3A02034789). The aerosol optical depth data and Angström Exponent data used in this study were obtained from http://ladsweb.nascom.nasa.gov/data/. Global Land Data Assimilation System (GLDAS) data used in this study were acquired as part of the mission of NASA's Earth Science Division and archived and distributed by the Goddard Earth Sciences (GES) Data and Information Services Center (DISC) (http://disc.sci.gsfc.nasa.gov/).

The Editor thanks Sagar Parajuli and an anonymous reviewer for their assistance in evaluating this paper.

References

Baddock, M. C., J. E. Bullard, and R. G. Bryant (2009), Dust source identification using MODIS: A comparison of techniques applied to the Lake Eyre Basin, Australia, *Remote Sens. Environ.*, *113*(7), 1511–1528, doi:10.1016/j.rse.2009.03.002.

Bangert, M., A. Nenes, B. Vogel, H. Vogel, D. Barahona, V. A. Karydis, P. Kumar, C. Kottmeier, and U. Blahak (2012), Saharan dust event impacts on cloud formation and radiation over Western Europe, *Atmo. Chem. Phys. Discuss.*, *11*(12), 31,937–31,982, doi:10.5194/acp-12-4045-2012.

Batjes, N. H. (2009), Harmonized soil profile data for applications at global and continental scales: Updates to the WISE database, *Soil Use Manage.*, *25*(2), 124–127, doi:10.1111/j.1475-2743.2009.00202.x.

Chen, Y., K. Yang, J. Qin, L. Zhao, W. Tang, and M. Han (2013), Evaluation of AMSR-E retrievals and GLDAS simulations against observations of a soil moisture network on the central Tibetan Plateau, *J. Geophys. Res. Atmos.*, *118*, 4466–4475, doi:10.1002/jgrd.00301.

Chomette, O., M. Legrand, and B. Marticorena (1999), Determination of the wind speed threshold for the emission of desert dust using satellite remote sensing in the thermal infrared, *J. Geophys. Res.*, *104*(D24), 31,207–31,215, doi:10.1029/1999JD900756.

Cowie, S. M., P. Knippertz, and J. H. Marsham (2013), Are vegetation-related roughness changes the cause of the recent decrease in dust emission from the Sahel?, *Geophys. Res. Lett.*, *40*, 1868–1872, doi:10.1002/grl.50273.

Crow, W. T., and D. Ryu (2009), A new data assimilation approach for improving runoff prediction using remotely-sensed soil moisture retrievals, *Hydrol. Earth Syst. Sci.*, *13*, 1–16, doi:10.5194/hess-13-1-2009.

Dong, Z., X. Liu, and X. Wang (2002), Wind initiation thresholds of the moistened sands, *Geophys. Res. Lett.*, *29*(12), 1585, doi:10.1029/2001GL013128.

Dorigo, W. A., K. Scipal, R. M. Parinussa, Y. Y. Liu, W. Wagner, R. A. M. De Jeu, and V. Naeimi (2010), Error characterisation of global active and passive microwave soil moisture datasets, *Hydrol. Earth Syst. Sci.*, *14*(12), 2605–2616, doi:10.5194/hess-14-2605-2010.

Eck, T. F., B. N. Holben, J. S. Reid, O. Dubovik, A. Smirnov, N. T. O'Neill, I. Slutsker, and S. Kinne (1999), Wavelength dependence of the optical depth of biomass burning, urban, and desert dust aerosols, *J. Geophys. Res.*, *104*(D24), 31,333–31,349, doi:10.1029/1999JD900923.

Engelstaedter, S., K. E. Kohfeld, I. Tegen, and S. P. Harrison (2003), Controls of dust emissions by vegetation and topographic depressions: An evaluation using dust storm frequency data, *Geophys. Res. Lett.*, *30*, 1294, doi:10.1029/2002GL016471.

FAO/IIASA/ISRIC/ISS-CAS/JRC (2009), *Harmonized World Soil Database (version 1.1)*, FAO, Rome, Italy.

Fécan, F., B. Marticorena, and G. Bergametti (1999), Parameterization of the increase of the aeolian erosion threshold wind friction velocity due to soil moisture for arid and semi-arid areas, *Ann. Geophys.*, *17*, 149–157, doi:10.1007/s00585-999-0149-7.

Gillette, D. A., J. Adams, D. Muhs, and R. Kihl (1982), Threshold friction velocities and rupture moduli for crusted desert soils for the input of soil particles into the air, *J. Geophys. Res.*, *87*(C11), 9003–9015, doi:10.1029/JC087iC11p09003.

Ginoux, P., J. M. Prospero, T. E. Gill, N. C. Hsu, and M. Zhao (2012), Global-scale attribution of anthropogenic and natural dust sources and their emission rates based on MODIS Deep Blue aerosol products, *Rev. Geophys.*, *50*, RG3005, doi:10.1029/2012RG000388.

Hsu, N. C., S. C. Tsay, M. D. King, and J. R. Herman (2004), Aerosol properties over bright-reflecting source regions, *Geosci. Remote Sens. IEEE Trans.*, *42*(3), 557–569, doi:10.1109/TGRS.2004.824067.

Ishizuka, M., M. Mikami, Y. Yamada, F. Zeng, and W. Gao (2005), An observational study of soil moisture effects on wind erosion at a gobi site in the Taklimakan Desert, *J. Geophys. Res.*, *110*, D18S03, doi:10.1029/2004JD004709.

Kaufman, Y. J., D. Tanré, and O. Boucher (2002), A satellite view of aerosols in the climate system, *Nature*, *419*(6903), 215–223, doi:10.1038/nature01091.

Kerr, Y. H., et al. (2010), The SMOS Mission: New tool for monitoring key elements of the global water cycle, *Proc. IEEE*, *98*(5), 666–687, doi:10.1109/JPROC.2010.2043032.

Kurosaki, Y., and M. Mikami (2003), Recent frequent dust events and their relation to surface wind in East Asia, *Geophys. Res. Lett.*, *30*(14), 1736, doi:10.1029/2003GL017261.

Kurosaki, Y., and M. Mikami (2007), Threshold wind speed for dust emission in East Asia and its seasonal variations, *J. Geophys. Res.*, *112*, D17202, doi:10.1029/2006JD007988.

Kurosaki, Y., M. Shinoda, and M. Mikami (2011), What caused a recent increase in dust outbreaks over East Asia?, *Geophys. Res. Lett.*, *38*, L11702, doi:10.1029/2011GL047494.

Kwon, H. J., S. H. Cho, Y. Chun, F. Lagarde, and G. Pershagen (2002), Effects of the Asian dust events on daily mortality in Seoul, Korea, *Environ. Res.*, *90*(1), 1–5, doi:10.1006/enrs.2002.4377.

Myhre, G., A. Grini, J. M. Haywood, F. Stordal, B. Chatenet, D. Tanré, J. K. Sundet, and I. S. A. Isaksen (2003), Modeling the radiative impact of mineral dust during the Saharan Dust Experiment (SHADE) campaign, *J. Geophys. Res.*, *108*(D18), 8579, doi:10.1029/2002JD002566.

Natsagdorj, L., D. Jugder, and Y. S. Chung (2003), Analysis of dust storms observed in Mongolia during 1937–1999, *Atmos. Environ.*, *37*(9), 1401–1411, doi:10.1016/S1352-2310(02)01023-3.

Parajuli, S. P., Z.-L. Yang, and G. Kocurek (2014), Mapping erodibility in dust source regions based on geomorphology, meteorology, and remote sensing, *J. Geophys. Res. Earth Surf.*, *119*, 1977–1994, doi:10.1002/2014JF003095.

Park, S. S., J. H. Kim, J. Lee, J. S. Kim, L. S. Chang, and S. Ou (2014), Combined dust detection algorithm by using MODIS infrared channels over East Asia, *Remote Sens. Environ.*, *141*, 24–39, doi:10.1016/j.rse.2013.09.019.

Prospero, J. M., P. Ginoux, O. Torres, S. E. Nicholson, and T. E. Gill (2002), Environmental characterization of global sources of atmospheric soil dust identified with the nimbus 7 total ozone mapping spectrometer (TOMS) absorbing aerosol product, *Rev. Geophys.*, *40*(1), 1002, doi:10.1029/2000RG000095.

Ravi, S., and P. D'Odorico (2005), A fieldscale analysis of the dependence of wind erosion threshold velocity on air humidity, *Geophys. Res. Lett.*, *32*, L21404, doi:10.1029/2005GL023675.

Ravi, S., P. D'Odorico, T. M. Over, and T. M. Zobeck (2004), On the effect of air humidity on soil susceptibility to wind erosion: The case of air-dry soils, *Geophys. Res. Lett.*, *31*, L09501, doi:10.1029/2004GL019485.

Rodell, M., et al. (2004), The global land data assimilation system, *Bull. Am. Meteorol. Soc.*, *85*(3), 381–394, doi:10.1175/BAMS-85-3-381.

Saxton, K. E., and W. J. Rawls (2006), Soil water characteristic estimates by texture and organic matter for hydrologic solutions, *Soil Sci. Soc. Am. J.*, *70*(5), 1569–1578, doi:10.2136/sssaj2005.0117.

Schepanski, K., I. Tegen, B. Laurent, B. Heinold, and A. Macke (2007), A new Saharan dust source activation frequency map derived from MSG-SEVIRI IR channels, *Geophys. Res. Lett.*, *34*, L18803, doi:10.1029/2007GL030168.

Sheffield, J., G. Goteti, and E. F. Wood (2006), Development of a 50-year high-resolution global dataset of meteorological forcings for land surface modeling, *J. Clim.*, *19*(13), 3088–3111, doi:10.1175/JCLI3790.1.

Sokolik, I. N. (2002), The spectral radiative signature of wind-blown mineral dust: Implications for remote sensing in the thermal IR region, *Geophys. Res. Lett.*, *29*(24), 2154, doi:10.1029/2002GL015910.

Sokolik, I. N., and O. B. Toon (1996), Direct radiative forcing by anthropogenic airborne mineral aerosols, *Nature*, *381*(6584), 681–683, doi:10.1038/381681a0.

Sun, J., M. Zhang, and T. Liu (2001), Spatial and temporal characteristics of dust storms in China and its surrounding regions, 1960–1999: Relations to source area and climate, *J. Geophys. Res.*, *106*(D10), 10,325–10,333, doi:10.1029/2000JD900665.

Tegen, I. (2003), Modeling the mineral dust aerosol cycle in the climate system, *Quat. Sci. Rev.*, *22*(18), 1821–1834, doi:10.1016/S0277-3791(03)00163-X.

Tegen, I., A. A. Lacis, and I. Fung (1996), The influence on climate forcing of mineral aerosols from disturbed soils, *Nature*, *380*(6573), 419–422, doi:10.1038/380419a0.

Tegen, I., M. Werner, S. P. Harrison, and K. E. Kohfeld (2004), Relative importance of climate and land use in determining present and future global soil dust emission, *Geophys. Res. Lett.*, *31*, L05105, doi:10.1029/2003GL019216.

Wang, X., Z. Dong, J. Zhang, and L. Liu (2004), Modern dust storms in China: An overview, *J. Arid Environ.*, *58*(4), 559–574, doi:10.1016/j.jaridenv.2003.11.009.

Zhang, Y., and G. R. Carmichael (1999), The role of mineral aerosol in tropospheric chemistry in East Asia—A model study, *J. Appl. Meteorol.*, *38*(3), 353–366.